

Supporting Information

Tuning the MnWO_4 Morphology and its Electrocatalytic activity towards Oxygen Reduction Reaction

Aarti Tiwari, Vikram Singh and Tharamani C. Nagaiah*

Department of Chemistry, Indian Institute of Technology Ropar, Rupnagar, Punjab-140001, India

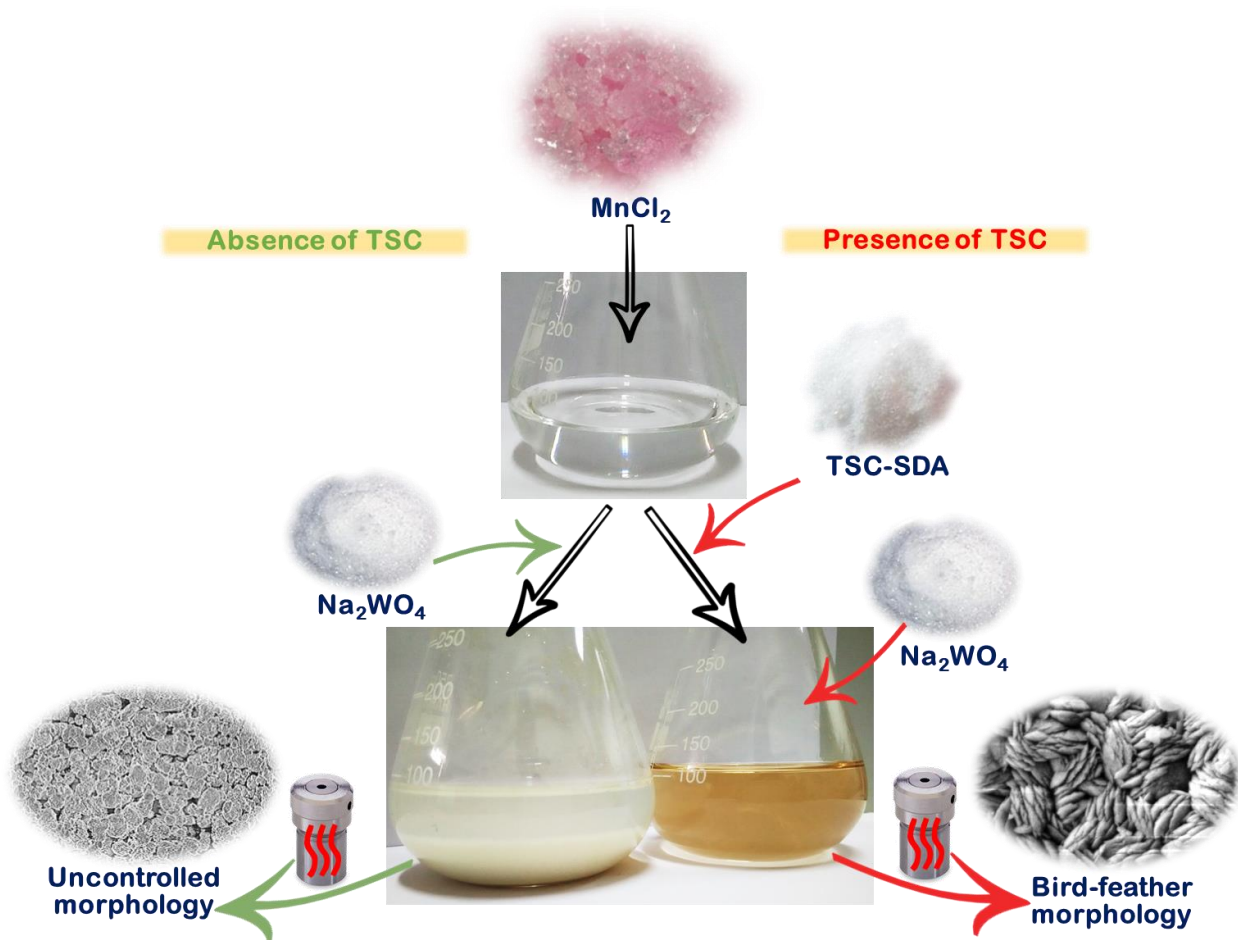


Fig. S1 Photographic image both in absence (left panel) and presence (right panel) of trisodium citrate (TSC) as a structure directing agent (SDA). Left panel shows immediate precipitation on mixing manganese chloride and sodium tungstate in absence of trisodium citrate. Right panel shows clear pale orange-brown color on mixing manganese chloride and sodium tungstate in presence of trisodium citrate due to complexing action. The bottom panel shows a comparative image of MnWO_4 for the absence and presence of TSC exhibiting the complexation-dependent effect.

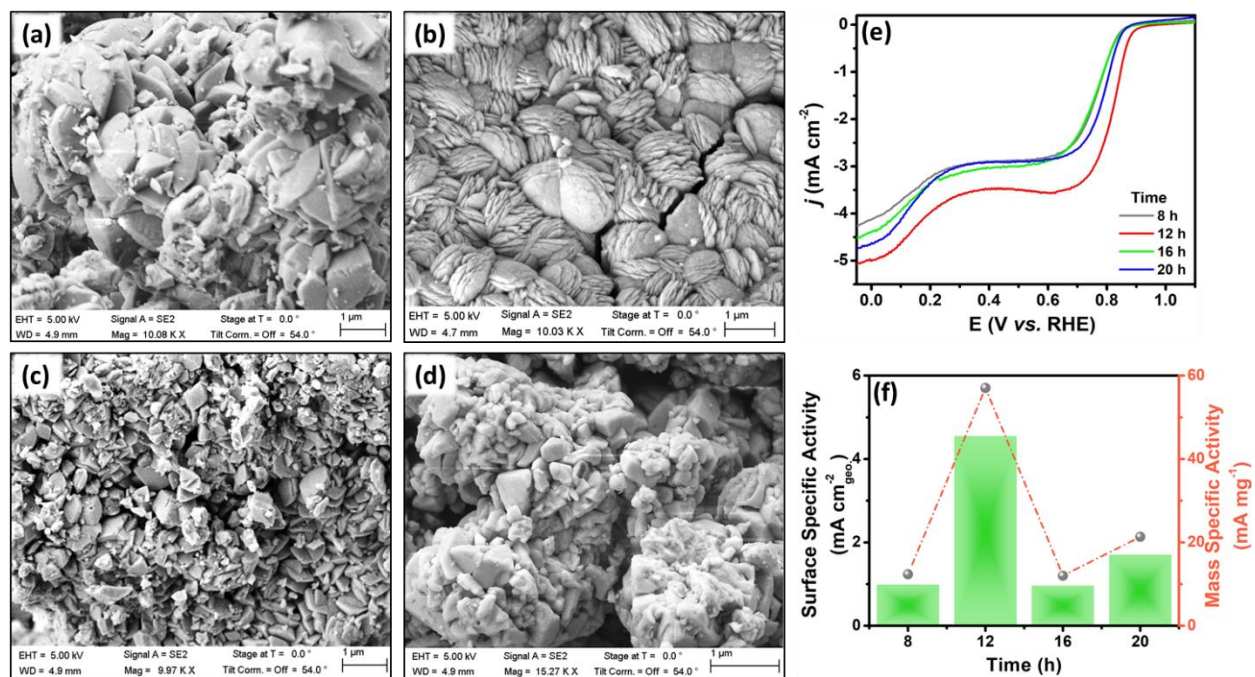


Fig. S2 FE-SEM images of MnWO₄ catalyst for different synthesis durations (a) 8 h, (b) 12 h, (c) 16 h and (d) 20 h; (e) The corresponding RDE polarization curves in O₂ saturated 1M NaOH and (f) Bar diagram representing the structure activity correlation extracted from RDE curves at 0.80 V with respect to surface specific activity and scatter plot for mass specific activity. CE: Pt-mesh; RE: Hg/HgO/1 M NaOH (Potentials converted to RHE).

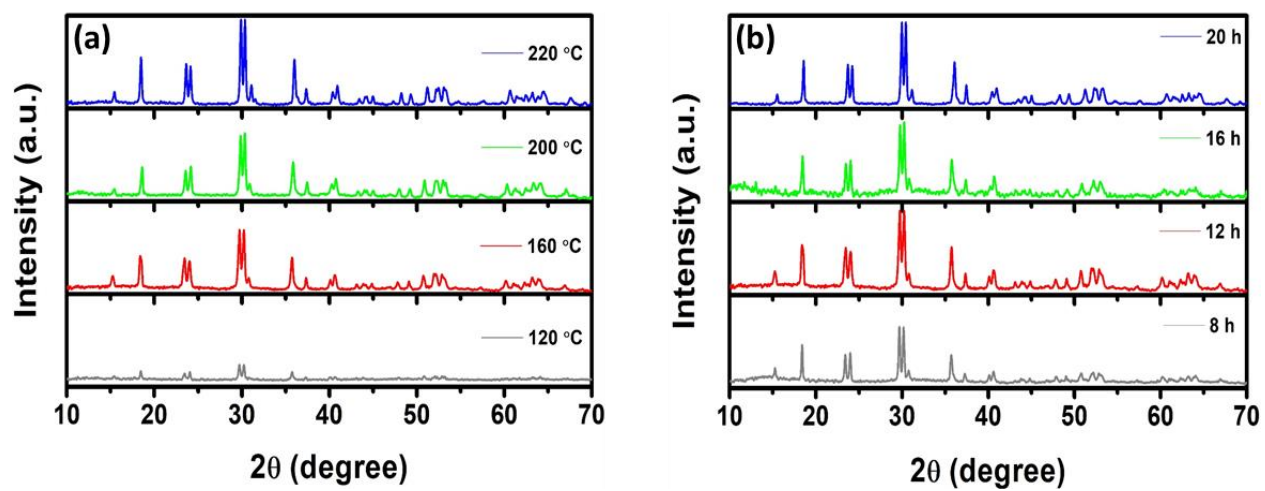


Fig. S3 XRD patterns of MnWO₄ for varying reaction (a) temperature and (b) time.

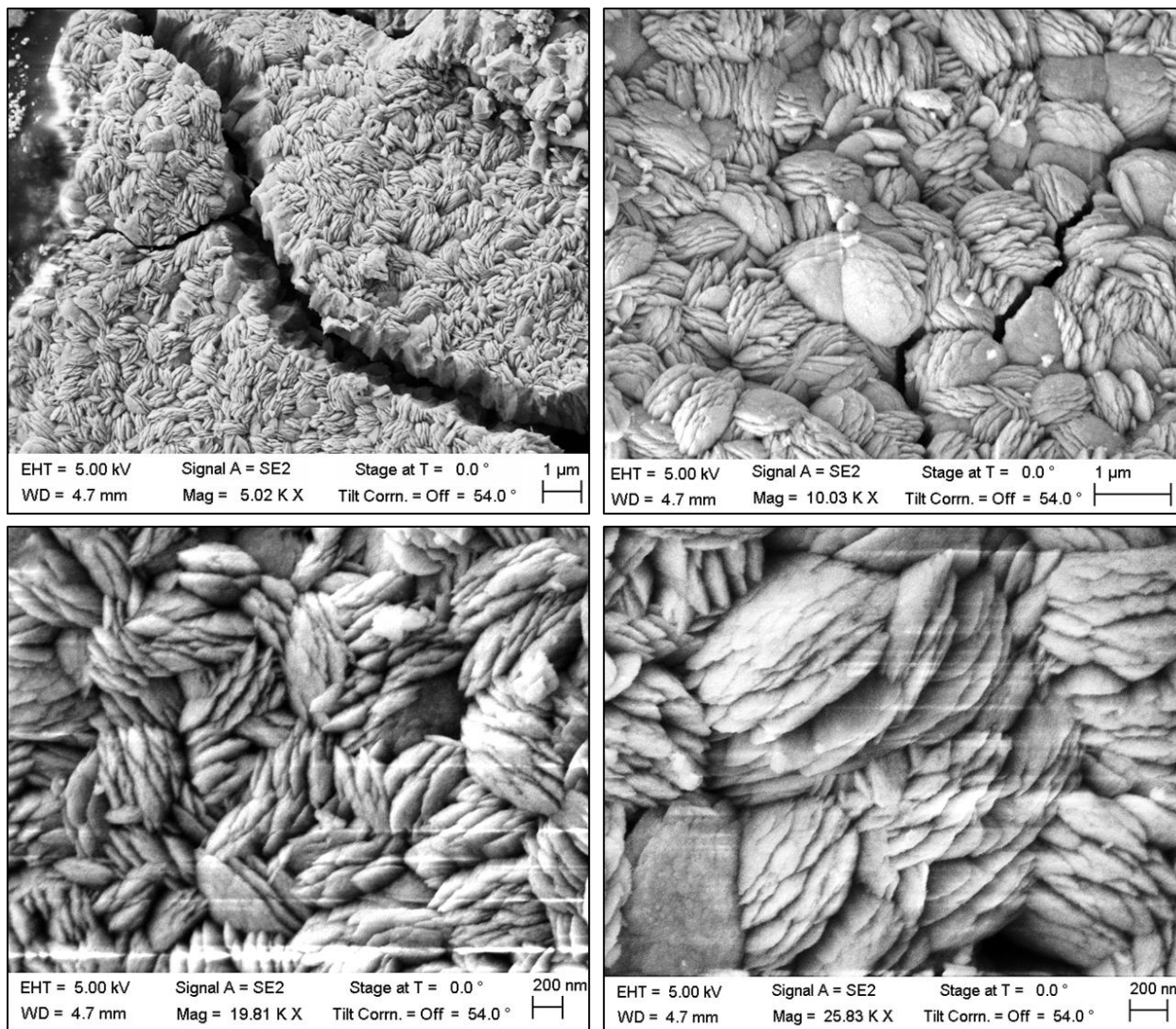


Fig. S4 FE-SEM images of MnWO₄-BF at different magnifications.

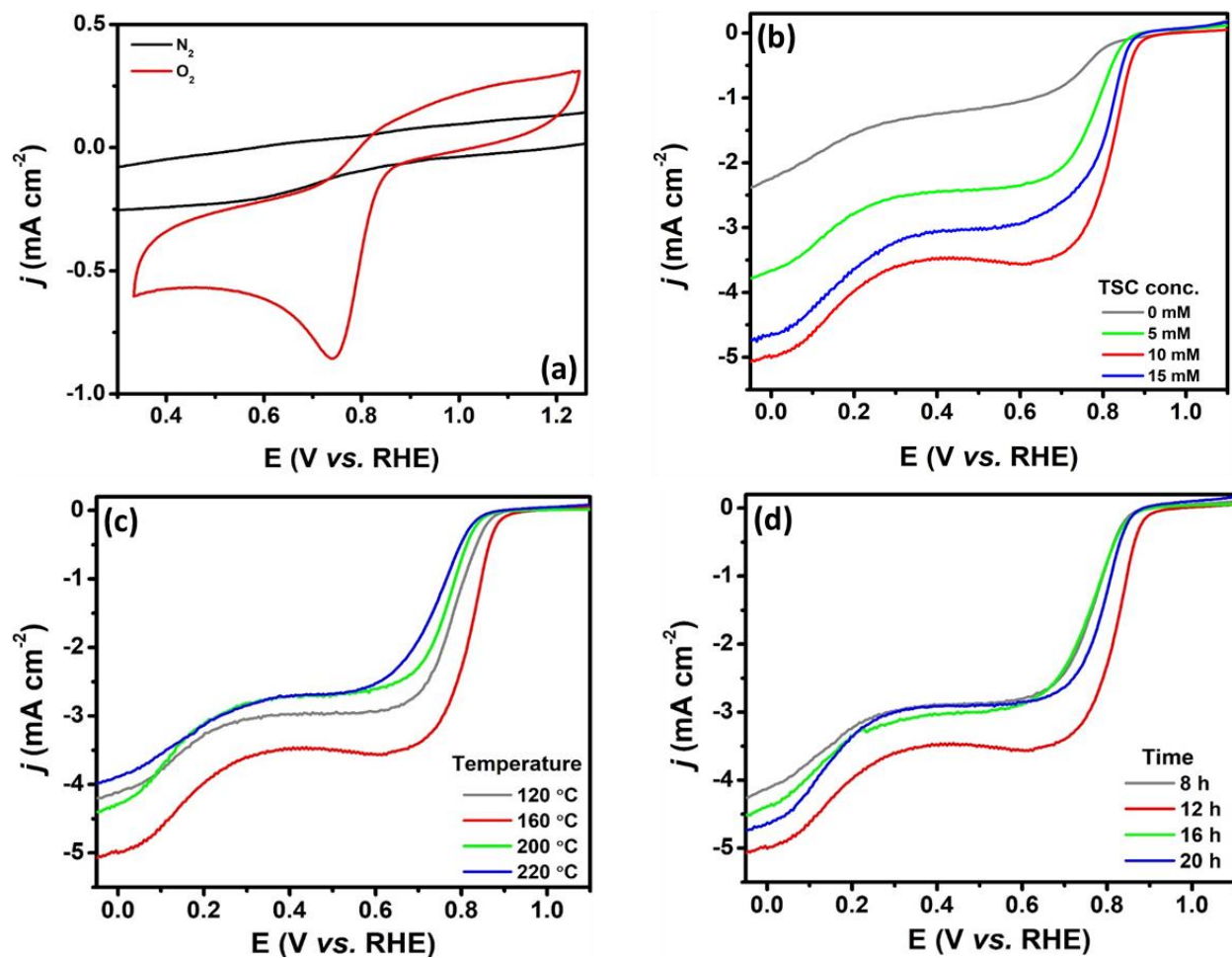


Fig. S5 Cyclic voltammograms for MnWO₄-BF recorded in both Ar and O₂-saturated 1 M NaOH electrolyte at a scan rate of 25 mV s⁻¹; RRDE polarization curves for varying (b) trisodium citrate (TSC) concentration; (c) temperature and (d) time at 1300 rpm in oxygen saturated 1 M NaOH at a scan rate of 5 mV s⁻¹. CE: Pt-mesh; RE: Hg/HgO/1 M NaOH (Potentials converted to RHE).

Table S1: Structure-activity correlation for MnWO₄.

Parameter	Variants	i_d at 0.1 V (mA cm ⁻²)	$i_{S.S.A}$ at 0.8 V (mA cm ⁻²)	$i_{M.S.A}$ at 0.8 V (mA cm ⁻²)
TSC conc.	0 mM	1.9	0.3	3.4
	5 mM	3.3	1.1	13.9
	10 mM	4.6	4.5	57.1
	15 mM	4.2	2.8	34.6
Temperature	120 °C	3.8	1.5	19.4
	160 °C	4.6	4.5	57.0
	200 °C	3.7	0.9	10.7
	220 °C	3.6	0.5	6.6
Time	8 h	3.7	1.0	12.4
	12 h	4.6	4.5	57.0
	16 h	3.9	1.0	12.0
	20 h	4.1	1.7	21.3

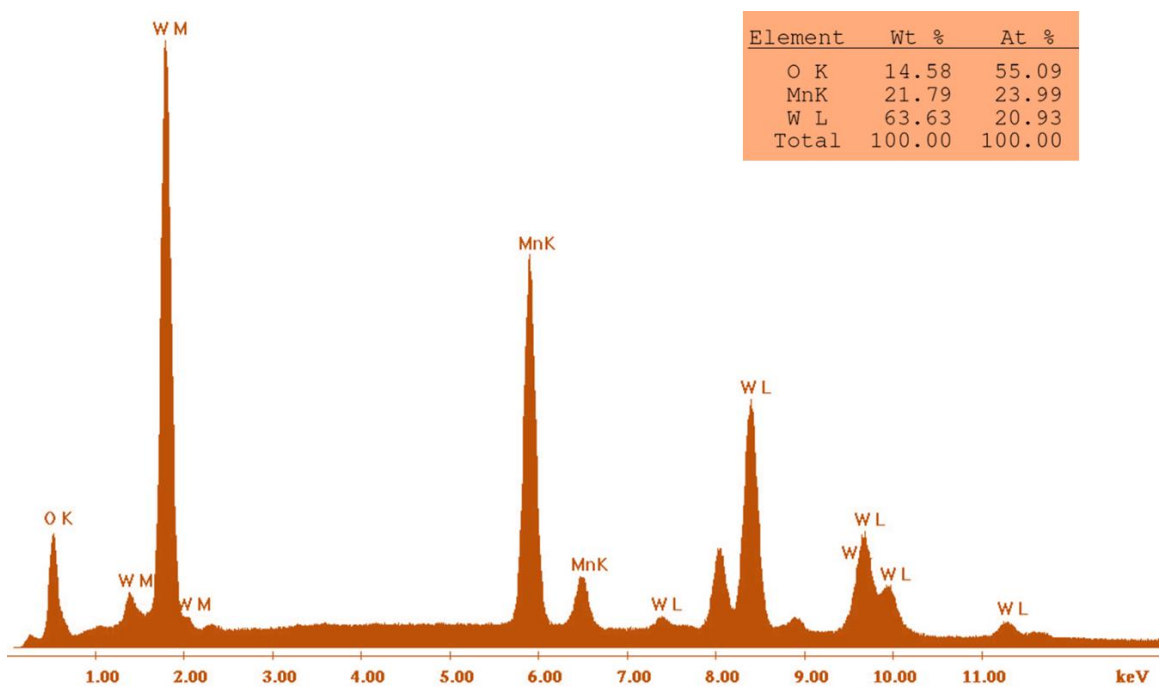


Fig. S6 EDX spectrum of MnWO₄-BF catalyst.

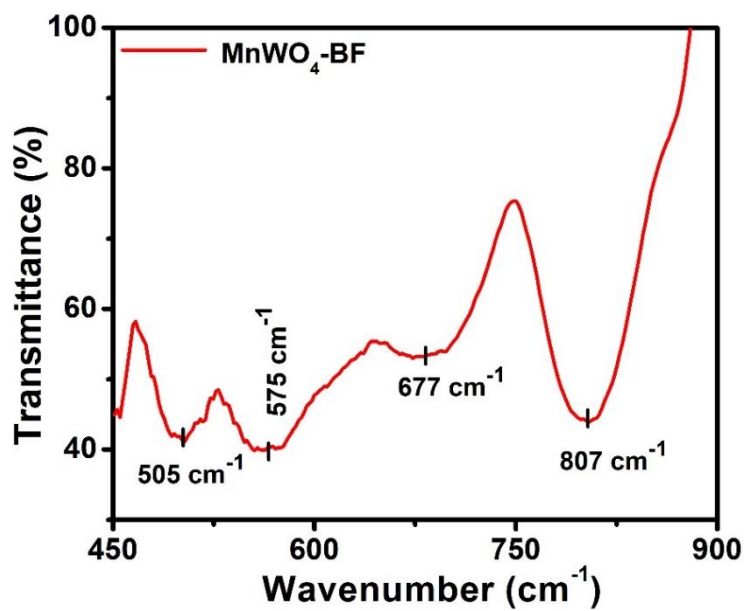


Fig. S7 FT-IR spectra of MnWO₄-BF catalyst.

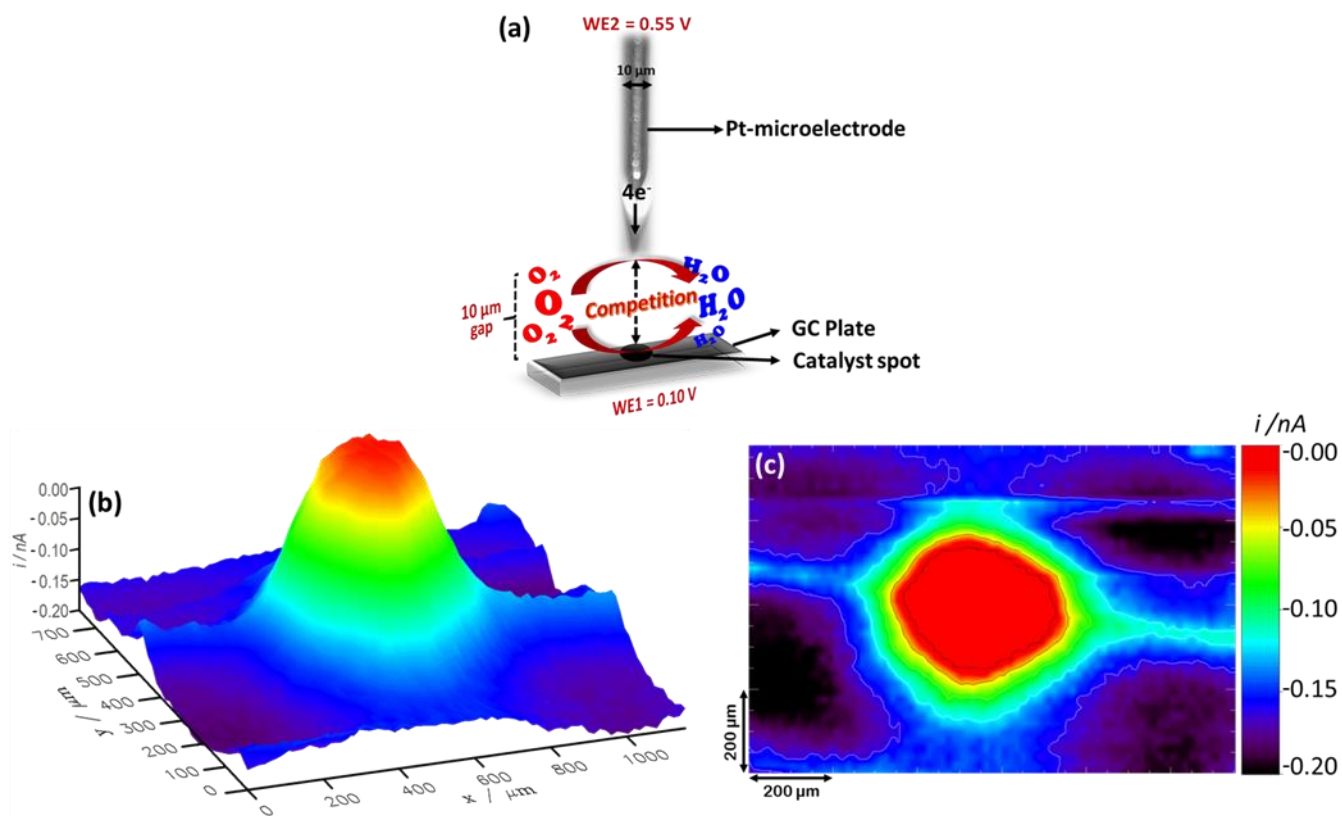


Fig. S8 (a) Schematic representation for RC-SECM mode with resultant (b) 3 D and (c) 2-D RC-SECM image of MnWO₄-BF catalyst where WE1 is polarized at 0.10 V while competing with Pt-tip (WE2 polarized at 0.55 V) for available dissolved oxygen in the gap between sample-to-tip in 0.1 M NaOH electrolyte. CE: Pt coil; RE: Ag/AgCl/3 M KCl (Potentials converted to RHE scale).

➤ RC-SECM analysis:

The ORR activity of various MnWO_4 catalysts prepared by varying the concentration of TSC-SDA was electrochemically imaged by employing redox-competition (RC) mode of scanning electrochemical microscopy (SECM) as illustrated in Fig. S9 (SI). This provides a surface map of catalytic activity to locate the *hot spots* i.e. the active site distribution using a bipotentiostatic 4-electrode configuration. Two working electrodes were employed where glassy carbon (GC) plate coated with MnWO_4 catalyst spots (0, 5, 10 and 15 mM variants) act as Working electrode 1 (WE1) while the other is Pt-ultramicroelectrode probe (\varnothing 10 μm) acting as WE2 which electrochemically scans to image a predefined region over WE1 spanning the catalysts. These two working electrodes were connected with a Pt coil counter electrode to complete the circuit while their potentials are referenced against Ag/AgCl/3M KCl (potentials converted to RHE scale) in O_2 saturated 0.1M NaOH electrolyte. The idea is to polarize both the working electrodes in their respective diffusion-limited regions so that they compete for the available dissolved oxygen in the 10 μm gap between the scanning plane of WE2 (fixed at 0.55 V) and catalyst surface (WE1). In order to trace the ORR activity, potential at WE1 was varied as 0.80, 0.55, 0.25 and 0.15 V in distinct RC-SECM scans.

The initial imaging was performed by polarizing WE1 at 0.80 V while WE2 at 0.55 V where the Pt-tip (WE2) acted as the probe whose current response was recorded while performing an x-y raster scan (2000 $\mu\text{m} \times 2000 \mu\text{m}$) 10 μm above the surface covering all the four catalyst spots. When the Pt-tip scans in RC mode the underlying catalytically active site rapidly consumes dissolved oxygen in the 10 μm gap between sample-to-tip so the ORR current at the Pt-tip decreases due to decreased oxygen availability. However, when the catalytically unmodified/inactive region is scanned the ORR current at the Pt-tip increases. These measured current responses at the Pt-tip is depicted as a surface plot in Fig. 4, S8 & S9 (SI) where the local catalytic activity is illustrated with a color scheme changing from blue to green through yellow to red with decreasing tip current which corresponds to a higher ORR electrocatalysis. All the four variants of TSC concentration (0, 5, 10 and 15 mM TSC) were simultaneously imaged to correlate their morphology with activity and emphasize the effect of a complexing TSC-SDA. As depicted by Fig. 4 (manuscript) electrocatalytic ORR activity over all these variants were scanned for sample potentials (WE1) ranging from kinetic-limited (0.80 V) to mass-transport limited (0.15 V) region following the trend 10 mM > 15 mM > 5 mM > 0 mM at all potentials. This was found to correspond well with the RDE derived specific activity (Fig. 4e). In order to further obtain a clear picture of obsolete tip current *versus* the catalyst spots at various WE1 potentials line scans (Y-axis; Fig. S10a-d, SI) passing through the center of catalyst spots were extracted from 3D RC-SECM scans represented in panels a-d of Fig. 4 (manuscript). This quantitatively reinforced the activity trend observed by qualitative 3D plots and a comparison of ORR activity as Y-line scans at different potentials is also depicted in Fig. S10e (SI) for the 10 mM TSC catalyst exhibiting BF morphology.

Besides, the distribution of ORR active sites over the catalyst surface was found to be more uniform for the 10 mM variant having the red regions spread all over the catalyst spot indicating maximum exposure of *hot spots* and hence the observed superior activity. Therefore, these microelectrochemical analysis suggest MnWO₄-BF synthesized using 10 mM TSC-SDA to have a superior ORR response in alkaline media which could be attributed to the uniform distribution of active sites over the catalyst surface as mapped by RC-SECM.

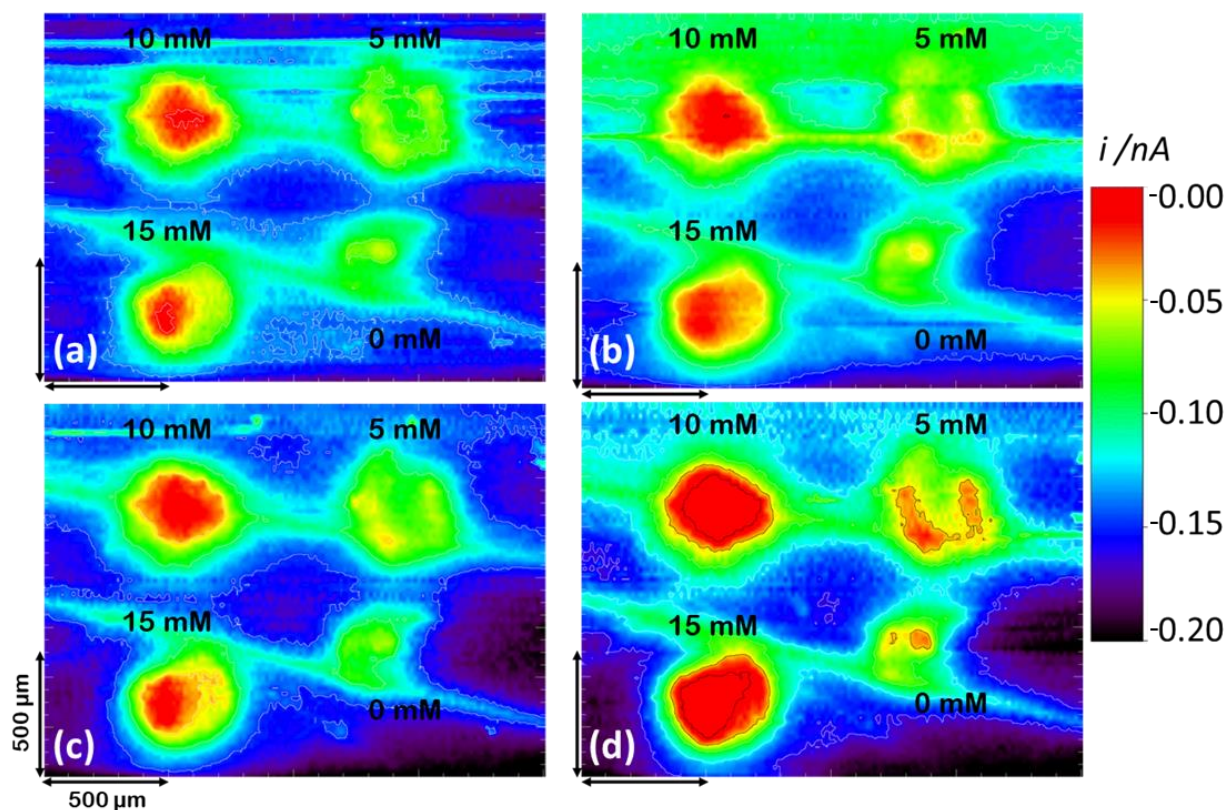


Fig. S9 2-D RC-SECM images of MnWO₄ catalyst at different TSC concentrations (0, 5, 10 and 15 mM) for varying WE1 potentials of (a) 0.80 V, (b) 0.55 V, (c) 0.25 V and (d) 0.15 V where WE2 was fixed at 0.55 V competing for the available dissolved oxygen in the gap between sample-to-tip in 0.1 M NaOH electrolyte. CE: Pt coil; RE: Ag/AgCl/3 M KCl (Potentials converted to RHE scale).

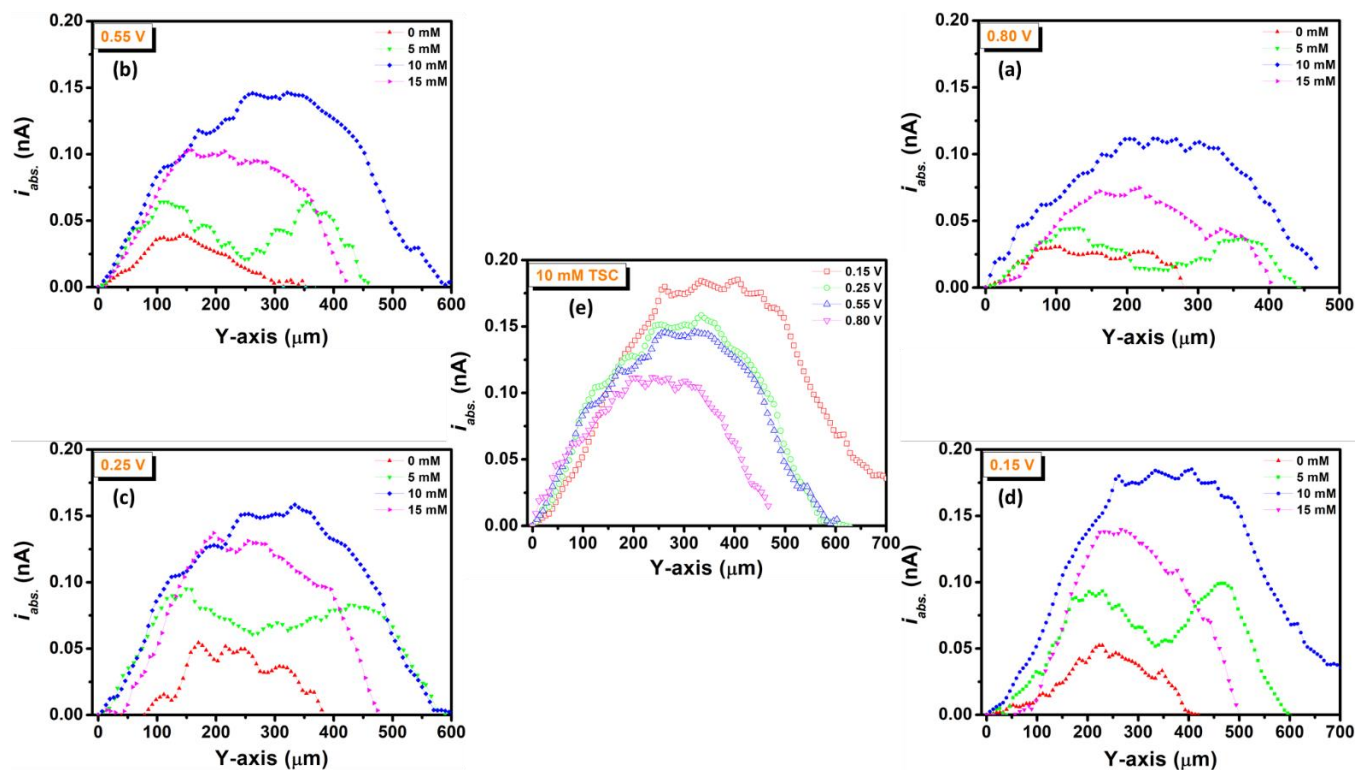


Fig. S10 (a) RC-SECM line scan (Y-axis) passing through the center of catalyst spots at (a) 0.80 V, (b) 0.55 V, (c) 0.25 V and (d) 0.15 V taken from panels a-d of Fig. 4 (manuscript) and (e) Comparison of 10 mM TSC catalyst spot upon varying WE1 potentials where WE2 was fixed at 0.55 V competing for the available dissolved oxygen in the 10 μm gap between sample-to-tip in 0.1 M NaOH electrolyte. CE: Pt coil; RE: Ag/AgCl/3 M KCl (Potentials converted to RHE scale).

➤ Sequential-pulse chronoamperometric SG-TC analysis:

A sequential-pulse chronoamperometry in sample-generation tip-collection (SG-TC) mode was performed to investigate ORR in-depth over MnWO₄-BF catalyst spot for both determination of onset potential and elucidation of mechanistic pathway. A 4-electrode setup was employed in the bipotentiostatic mode comprising of two working electrodes (WE), MnWO₄-BF coated onto glassy carbon plate (WE1) was placed at the bottom of the cell whereas Pt-ultramicroelectrode (\varnothing 10 μ m) acts as WE2 placed 10 μ m above WE1 and are referenced against Ag/AgCl/3M KCl using Pt coil as the counter electrode. Herein as the name of the mode suggests, WE1 acts as the *generator* which performs the main reaction of interest *i.e.* ORR generating intermediates which are collected at the WE2 *collector*. The chronoamperometric pulse profiling was programmed so that WE2 was constantly polarized at 1.4 V to detect the formation of even trace amount of H₂O₂ intermediate (by oxidizing it back to O₂) while the potential was varied at WE1 from 1.19 V to -0.21 V with a step potential of -0.05 V after every 2 min. to invoke ORR for process analysis. So, the first potential applied at WE1 was 1.19 V while WE2 was fixed at 1.4 V and the current response was recorded at both WE1 and WE2 for 2 min. Subsequently, the WE1 potential was stepped down by 0.05 V cathodically to 1.14 V (while WE2 remains fixed at 1.4 V) and again the observed current response was recorded at both the working electrodes for 2 min. This process was continued till WE1 potential reached -0.21 V. The data of this overall chronoamperometric measurement is represented in Fig. 5a (manuscript) where the top section depicts oxidation current at WE2 for any intermediate H₂O₂ detection, recorded in response to cathodically pulsing the potential (from 1.19 V to -0.21 V) at catalyst spot (WE1) as shown in the bottom section.

The chronoamperometric SG-TC response illustrated in Fig. 5a (manuscript) depicts colored arrows in the bottom section denoting each potential step and its corresponding tip response is traced in the top section with the same color. So, the first black arrow in the bottom section denotes O₂ reduction current response (if any) for application of 1.19 V at WE1 and simultaneously the top section represents H₂O₂ oxidation current response (if any) by application of constant 1.4 V at WE2 for 2 min. *i.e.* duration of the first chronoamperometric pulse. Subsequently, the potential at WE1 was stepped down by 50 mV to 1.14 V while the potential at WE2 remained fixed at 1.4 V and the respective WE1 and WE2 current response for the second 2 min. pulse is represented in red color and so on till WE potential reached -0.21 V.

Evidently, the first dip in WE1 reduction current starts from 0.99 V (cyan color), marking the ORR onset with a simultaneous increase in oxidative current at the WE2 Pt-tip, confirming the initial formation of peroxide species. Such a precise H₂O₂ detection was facilitated only due to the miniaturization of Pt-tip probe (\varnothing 10 μ m) and the micrometric sample-to-tip distance (10 μ m). This response *i.e.* increasing ORR current (negative current for WE1) and increasing H₂O₂ oxidation current (positive current for WE2) continued till 0.79 V. Thereafter, WE2 oxidative current remained nearly constant till 0.29 V which subsequently decreases upon stepping to more cathodic potentials (*i.e.* 0.24 to -0.21 V). This decrease in H₂O₂ oxidation current beyond

0.24 V occurs due to complete conversion of O_2 to H_2O at the catalyst (WE1) which in turn increases the WE1 reduction current and since there is no further generation of H_2O_2 the corresponding current at WE2 decreases. Therefore, the oxygen reduction current increased (became more negative at WE1) upon pulsing to more negative potentials (from 1.19 to -0.21 V) whereas the intermediate generation decreased due to complete $4 e^-$ reduction thereby decreasing the concentration of H_2O_2 which is responsible for decrease in oxidative current at WE2.

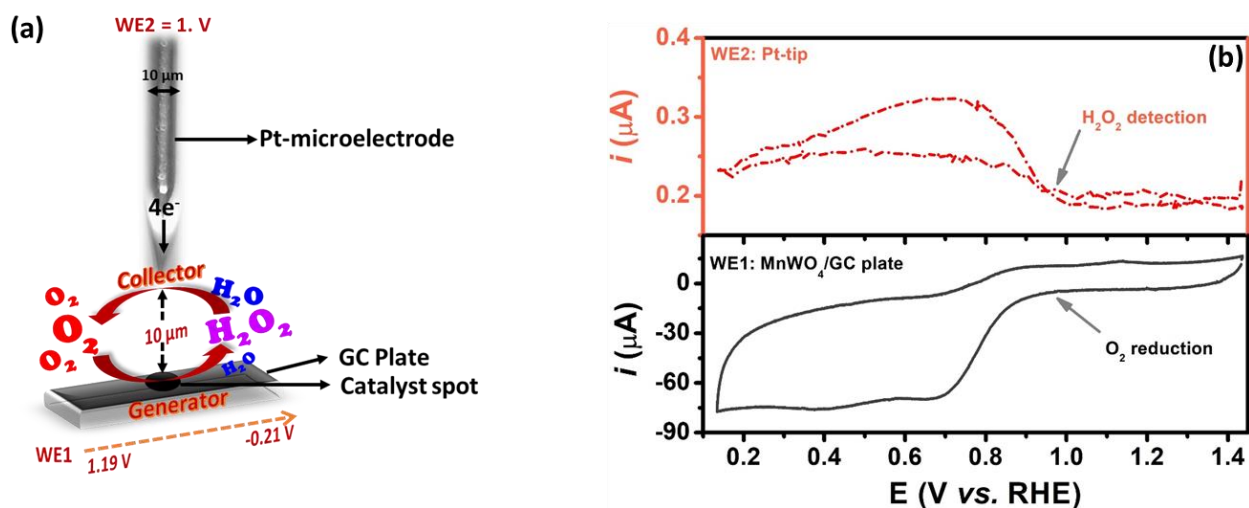


Fig. S11 (a) Schematic representation for SG-TC mode of SECM and (b) corresponding SG-TC cyclic voltammogram obtained by constantly polarizing WE2 at 1.4 V while scanning WE1 from 1.4 V to 0.1 V at 25 mV s^{-1} in O_2 saturated 1 M NaOH electrolyte. CE: Pt coil; RE: Ag/AgCl/3 M KCl (Potentials converted to RHE scale).

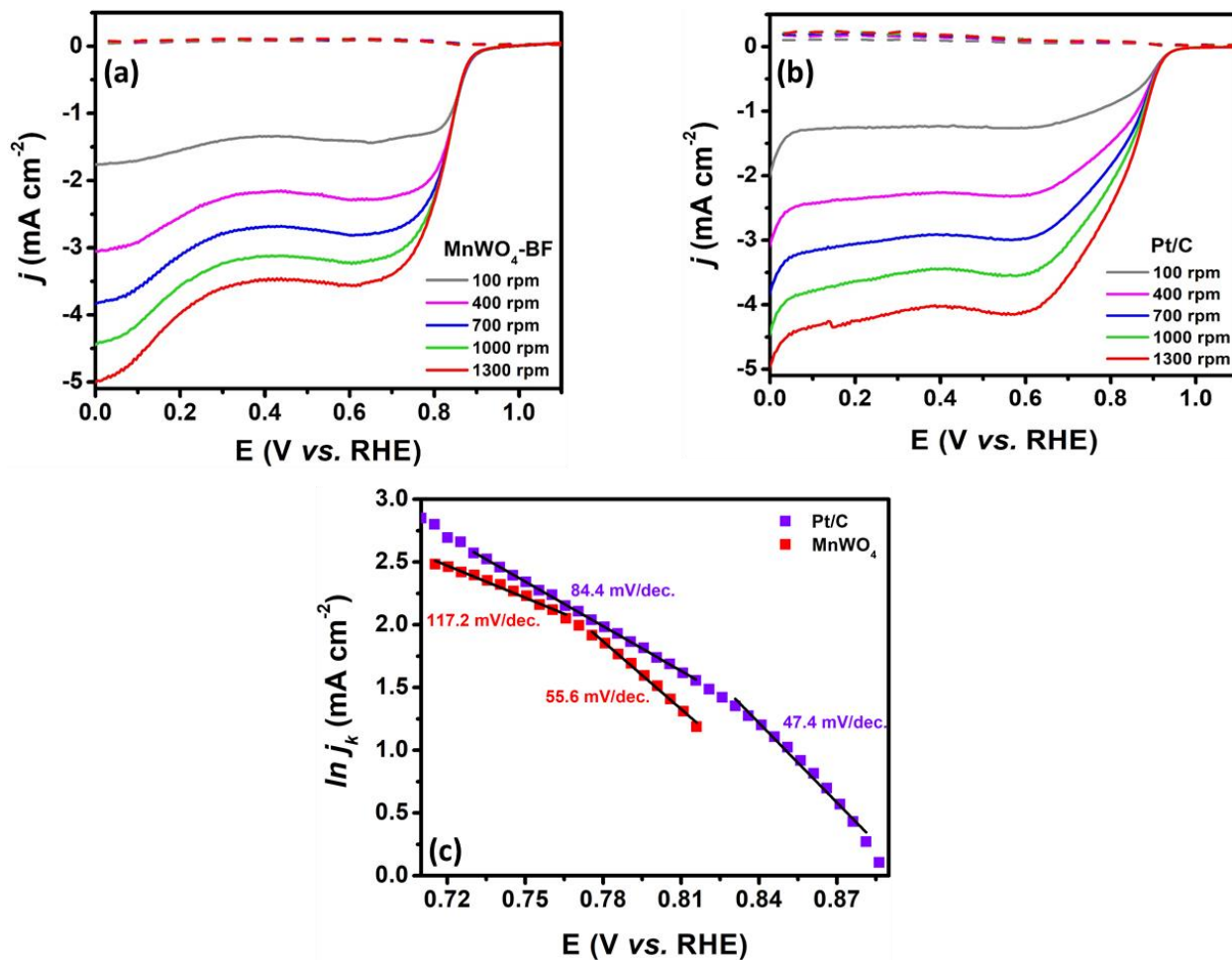


Fig. S12 Rotating ring-disk voltammograms at varying rotation rates in oxygen saturated 1 M NaOH for (a) MnWO₄-BF and (b) Pt/C (20%) catalysts at a scan rate of 5 mV s⁻¹ and (c) corresponding Tafel slope in the kinetic-limited potential range. CE: Pt-mesh; RE: Hg/HgO/1 M NaOH. (Potentials converted to RHE scale)

➤ **Koutecky-Levich Analysis:**

The linear polarization curves recorded by performing rotating disk electrode (RDE) analysis for different TSC concentration, temperature and time are represented in Fig. S5. These can be further utilized to estimate the number of electrons (n) transferred for undergoing oxygen reduction by using Koutecky-Levich equation¹:

$$\frac{1}{j} = \frac{1}{j_d} + \frac{1}{j_k} = \frac{1}{B\sqrt{\omega}} + \frac{1}{j_k} \quad (1)$$

Where, ' j ' is the measured current density denoted as ' j_d ' for diffusion/mass transport limited current density and ' j_k ' is the kinetic current density. The term ' ω ' is the angular rotation rate of the electrode where ' B ' can be defined as¹:

$$B = 0.62 n F A D^{2/3} \gamma^{-1/6} C \quad (2)$$

Where, ' n ' is the number of electrons, ' F ' is the Faraday constant (96500 C/mol), ' A ' is the area of the electrode (here, 0.1256 cm²), ' D ' is the oxygen diffusion coefficient (1.43 x 10⁻⁵ cm²/s), ' γ ' is the kinematic viscosity of the electrolyte (1.13 x 10⁻² cm²/s) and ' C ' is the bulk concentration of oxygen in the electrolyte medium (0.843 x 10⁻⁶ mol/cm³).

In order to estimate the number of electrons (n) transferred, a plot between $1/j$ vs. $1/\sqrt{\omega}$ was constructed as shown in Fig. S13. The slope of this K-L plot gives ' $1/B$ ' which is further used to calculate the potential dependent transfer of electrons as detailed in Table S2.

Table S2: Koutecky-Levich Analysis.		
Potential Applied (V vs. RHE)	No. of electrons (n)	
	MnWO₄-BF	Pt/C (20%)
0.1	4.0	3.7
0.2	3.9	3.7
0.3	3.6	3.7
0.4	3.5	3.6

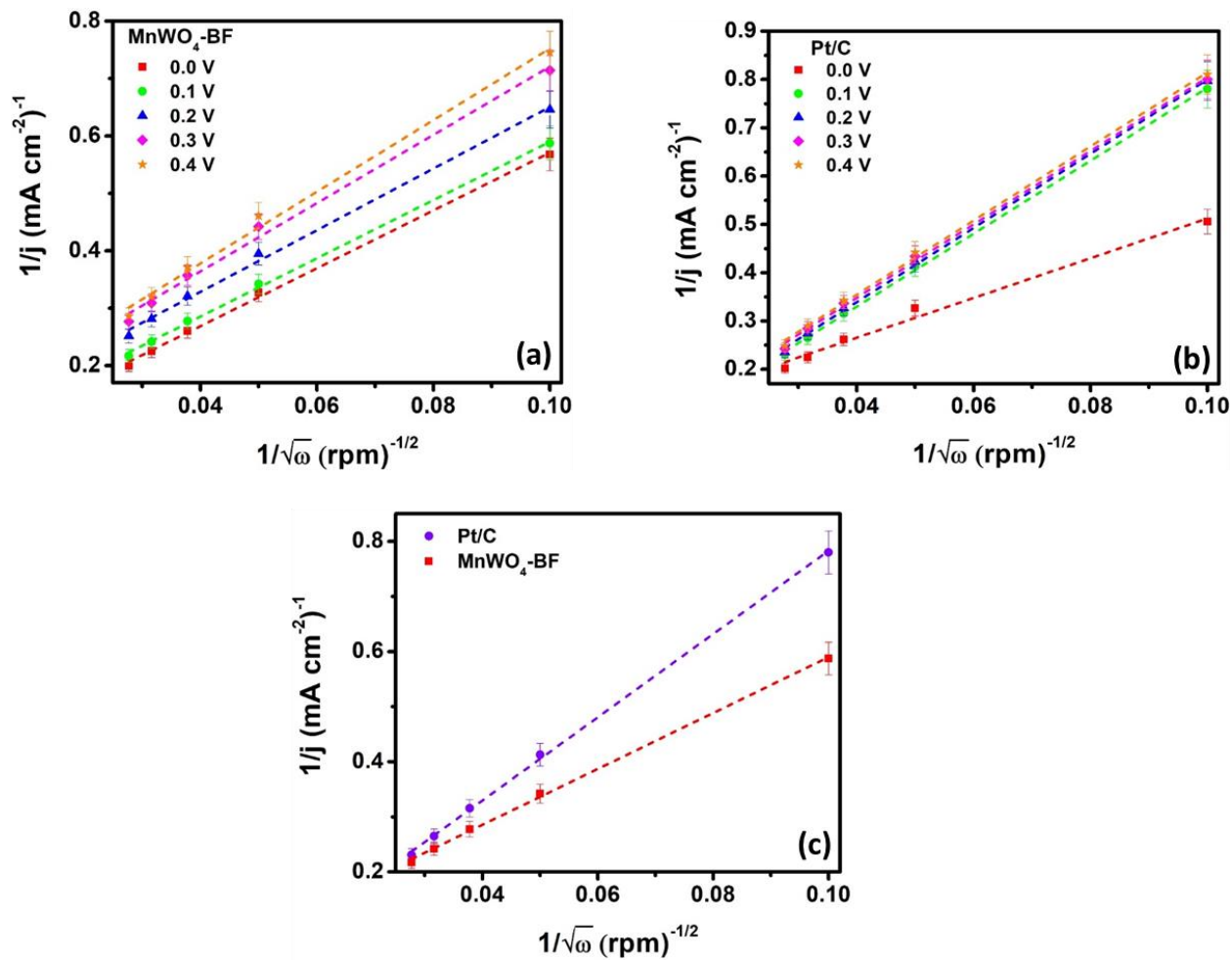


Fig. S13 Koutecky-Levich plot for (a) MnWO₄-BF and (b) Pt/C (20%) catalysts at varying potentials derived from the linear polarization curves (Fig. S12) at different rotation rates and (c) comparison of MnWO₄-BF with Pt/C (20%) at 0.1 V. (Potentials converted to RHE scale)

➤ **Rotating ring-disk Analysis:**

The RRDE polarization curves recorded in 1 M NaOH at 5 mV s⁻¹ in the potential range of 1.1 V to 0.0 V were evaluated to estimate the number of electrons transferred '*n*' and percentage of H₂O₂ produced (% H₂O₂) as follows²;

$$n = 4 I_d \left[I_d + \left(\frac{I_r}{N} \right) \right] \quad (1)$$

$$\% H_2O_2 = 200 \times (I_r/N) / \left[I_d + \left(\frac{I_r}{N} \right) \right] \quad (2)$$

Where, '*I_d*' and '*I_r*' denote the disk and the ring currents respectively whereas '*N*' is the collection efficiency of the ring determined to be 0.38 by performing RRDE measurements in a [Fe(CN)₆]^{4-/3-} redox medium. The potential dependent variation of '*n*' and %H₂O₂ for both the catalysts are represented in Fig. 5c (detailed in Table S3) showing nearly 2 e⁻ transfer and ca. 70% peroxide production for MnWO₄-BF whereas 3 e⁻ transfer with ca. 40% H₂O₂ formation for Pt/C (20%). But cathodically increasing the potential leads to an increase in electron transfer number (*n*) which slightly decreases after 0.5 V for Pt/C (20%) with a simultaneous increase in peroxide content in contrast to MnWO₄. At 0.1 V, mass transfer governs the ORR process and MnWO₄ overtakes Pt/C (20%) with '*n*' as 3.8 and %H₂O₂ as 8% in contrast to '*n*' of 3.5 with 25% H₂O₂ respectively which is in coherence with the K-L analysis.

Tafel analysis was also performed by plotting logarithmic kinetic current density (*j_k*, obtained by normalizing kinetic current; $I_k = \frac{I_{lim.} \times I}{I_{lim.} - I}$ w.r.t. geometric surface area where, '*I*' is the measured current and '*I_{lim.}*' is the diffusion limited current)² against potential shown in Fig. S12c to hint the kinetically predominant ORR pathway. Tafel slope was found to decrease progressively upon decreasing the cathodic potential (*i.e.* overpotential) which is generally attributed to the significant surface oxide and hydroxide coverage. The comparatively small Tafel slope value for Pt/C (20%) at low overpotentials (*η*) signifies decrease in apparent active area for O₂ adsorption limiting its kinetics in alkaline media.

Potential Applied (V vs. RHE)	MnWO ₄ -BF		Pt/C (20%)	
	<i>n</i>	% H ₂ O ₂	<i>n</i>	% H ₂ O ₂
0.1	3.8	8.6	3.5	24.6
0.3	3.7	14.3	3.4	27.5
0.5	3.7	14.8	3.6	16.5
0.7	3.7	14.7	3.7	12.1
0.9	2.6	68.2	3.3	35.1

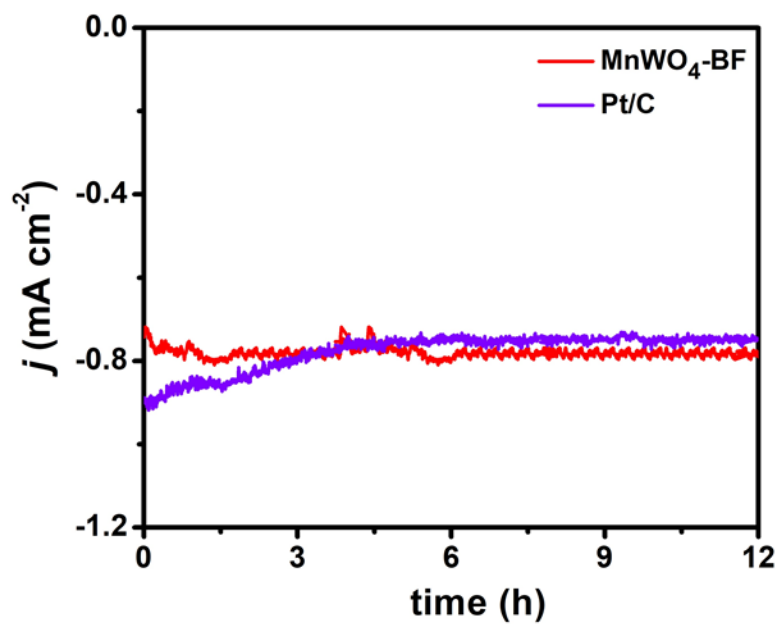


Fig. S14 Chronoamperometric ORR stability analysis of MnWO₄-BF against Pt/C (20%) in oxygen saturated 1 M NaOH at 0.23 V for 12 h. CE: Pt mesh; RE: Hg/HgO/1M NaOH (Potentials converted to RHE scale).

➤ **Electrochemical surface area analysis:**

Electrochemical active surface area (ECSA) was determined by evaluating double-layer capacitance measurements. A series of cyclic voltammograms were recorded at different scan rates varying from 10 to 320 mV s^{-1} in a non-faradaic potential range *i.e.* 0.1 to -0.1 V (vs. Hg/HgO/1M NaOH) in 1 M NaOH electrolyte. The obtained response was therefore ascribed to have origin only in the capacitance behavior of the electrocatalytic system. A plot between the average current density $[(I_a+I_c)/2]$; where 'a' denotes anodic current and 'c' is for cathodic current at 0 V (vs. Hg/HgO)] vs. the scan rate results in a linear graph, the slope of which gives double-layer pseudo-capacitance ($C_{dl} = 2 \times 10^{-4} \text{ F cm}^{-2}$). Subsequently dividing this C_{dl} with specific capacitance for a planar surface ($40 \times 10^{-6} \text{ F cm}^{-2}$)³ yields ECSA to be 5 cm^2 . Normalizing ECSA with the catalyst loading ($9 \mu\text{g}$ over $\varnothing 3 \text{ mm}$ GC) gave a very high specific electrochemical surface area (SESA) of $45 \text{ m}^2 \text{ g}^{-1}$ which is strikingly at par with Pt/C (20%) having $48 \text{ m}^2 \text{ g}^{-1}$ SESA.²

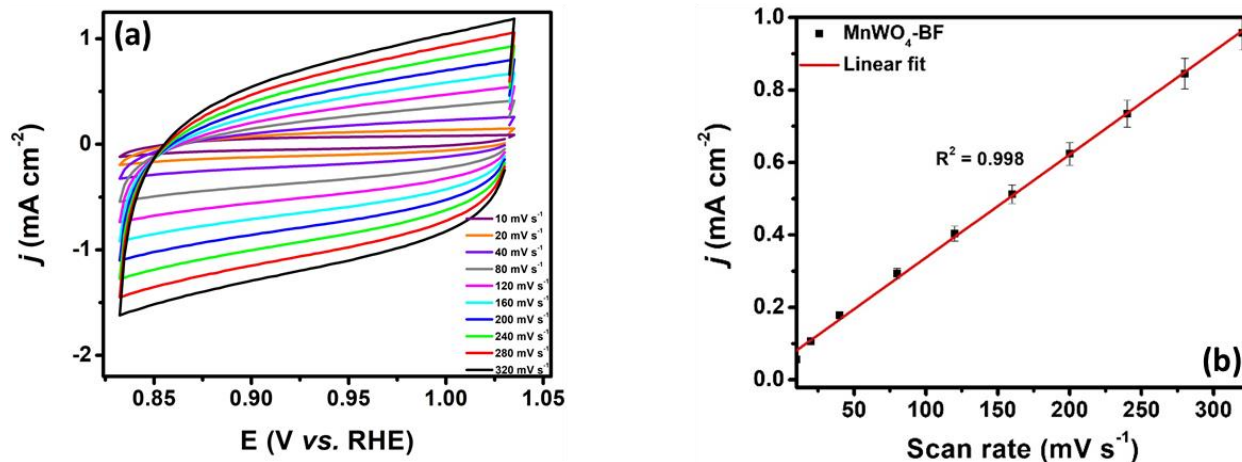


Fig. S15 Cyclic voltammogram in the non-faradic potential region at varying scan rates and the corresponding plot of average current density vs. scan rate for MnWO₄-BF in 1 M NaOH electrolyte. CE: Pt-mesh; RE: Hg/HgO/1 M NaOH (Potentials converted to RHE).

Table S4: ECSA Analysis.		
TSC conc. (mM)	ECSA (cm^2)	Specific surface area (m^2/g)
0	0.6	5.4
5	1.8	16.2
10	5.0	45.0
15	3.3	29.7

Table S5: ORR performance of Mn-based electrocatalysts in alkaline medium.			
Catalyst	Synthetic approach	E_{onset} (V vs. RHE)	Ref.
Pt/C (20 wt%)	E-TEK	1.07	4
Pt/VC	Commercial	0.93	5
Mn ₃ O ₄ /pGC	Sputtering over GC	0.85	6
MnO _x /PEDOT	Electro deposition over PEDOT	0.87	7
MnO ₂ /C	Hydrothermally	0.06 vs. Ag/AgCl	8
Mn ₃ O ₄ /N/C	Calcination, hydrothermal and pyrolysis at 1000° C	0.91	9
MnO ₂ -NWs@Ni-NPs/C	Hydrothermally and Calcination	0.08 vs. Ag/AgCl	8
Hierarchical MnO ₂ /reduced graphene oxide	Solution phase	-0.176 vs. SCE	10
α-MnO ₂ -SF	solid state method	-0.13 vs. SCE	11
MnO ₂ + MOF(Fe)	Hydrothermal treatment	0.84	12
MnWO₄-BF	Complexation precipitation	0.99	Present work

References:

1. A. Tiwari and T. C. Nagaiah, *ChemCatChem*, 2016, **8**, 396-403.
2. A. Tiwari, V. Singh, D. Mandal and T. C. Nagaiah, *J. Mater. Chem. A*, 2017, **5**, 20014-20023.
3. V. Singh, S. D. Adhikary, A. Tiwari, D. Mandal and T. C. Nagaiah, *Chem. Mater.*, 2017, **29**, 4253-4264.
4. J. Perez, E. R. Gonzalez and E. A. Ticianelli, *Electrochim. Acta*, 1998, **44**, 1329-1339.
5. R. Jäger, E. Härk, P. E. Kasatkin and E. Lust, *J. Electrochem. Soc.*, 2014, **161**, F861-F867.
6. Y. Gorlin, C.-J. Chung, D. Nordlund, B. M. Clemens and T. F. Jaramillo, *ACS Catal.*, 2012, **2**, 2687-2694.
7. J. A. Vigil, T. N. Lambert and K. Eldred, *ACS Appl. Mater. Interfaces*, 2015, **7**, 22745-22750.
8. F. Cheng, Y. Su, J. Liang, Z. Tao and J. Chen, *Chem. Mater.*, 2010, **22**, 898-905.
9. S. Gao and K. Geng, *Nano Energy*, 2014, **6**, 44-50.
10. D. Guo, S. Dou, X. Li, J. Xu, S. Wang, L. Lai, H. K. Liu, J. Ma and S. X. Dou, *Int. J. Hydrogen Energy*, 2016, **41**, 5260-5268.
11. Y. Meng, W. Song, H. Huang, Z. Ren, S.-Y. Chen and S. L. Suib, *J. Am. Chem. Soc.*, 2014, **136**, 11452-11464.
12. H. Wang, F. Yin, B. Chen and G. Li, *J. Mater. Chem. A*, 2015, **3**, 16168-16176.